Grid-independent large-eddy simulation in turbulent channel flow using three-dimensional explicit filtering

By Jessica Gullbrand

1. Motivation and objectives

In traditional large-eddy simulation (LES) solution methods, the computational grid and discretization operators are considered as "implicit" filtering of the Navier-Stokes equations. This LES procedure divides the turbulent flow field into resolved and unresolved scales, where the unresolved scales must be modeled.

When explicit filtering is used in LES, the filtering procedure of the governing equations is separated from the grid and discretization operations. This separation now divides the flow field into resolved filtered scale (RFS) motions, and subfilter-scale (SFS) motions. The SFS is itself divided into a resolved part (RSFS) and an unresolved part (USFS) (Zhou, Brasseur & Juneja 2001): see figure 1. The RFS motion is obtained by solving the filtered Navier-Stokes equations. The RSFS motions can theoretically be reconstructed from the resolved field and occur due to the use of a smooth (in spectral space) filter function. The USFS motions consist of scales that are not resolved in the simulation and need to be modeled. The explicitly-filtered governing equations were recently studied by Carati, Winckelmans & Jeanmart (2001).

The smallest resolved scales are often used to model the turbulence-closure term in LES, and therefore it is of great importance to capture these scales to high accuracy. The accuracy of the LES solution can be increased by using high-order numerical schemes. High-order methods will increase the accuracy of the important large energy-containing scales, but the small scales will still be contaminated with truncation errors when using non-spectral methods. These errors can be reduced or eliminated by using explicit filtering in LES (Lund 1997). This can be achieved either by using a large ratio between the filter width and the cell size, or by using a higher-order method, then the ratio need not be so large. In recent *a priori* studies by Chow & Moin (2003), a minimum ratio of filter width to cell size was determined to prevent the numerical error from becoming larger than the contribution from the turbulence closure term. They concluded that a fourth-order scheme should be used with a filter width of at least twice the cell size, and for a second-order scheme the filter width should be at least four times the cell size.

Using explicit filtering and high-order numerical schemes requires the filter functions to be commutative to at least the same order as the numerical scheme. The differentiation and the filtering operations must commute, to ensure that the filtered Navier-Stokes equations have the same structure as the unfiltered equations. In general, the operations do not commute when a variable filter width is used, as is needed in inhomogeneous flow fields. Ghosal & Moin (1995) showed that the commutation error is of the same order as the contribution from the turbulence closure term, $O(\Delta^2)$, where Δ is the filter width. Therefore, this error must be reduced or eliminated to avoid significant effects on the

LES solution. A general theory for constructing discrete high-order commutative filters was proposed by Vasilyev, Lund & Moin (1998).

Most previous studies of LES using explicit filtering in turbulent channel flow have used filtering in two dimensions (the homogeneous directions) and only a few studies have applied filtering in all three dimensions. Only investigations performed using smooth filter functions are discussed here. Two-dimensional filtering was investigated by Piomelli, Moin & Ferziger (1988), Najjar & Tafti (1996), Sarghini, Piomelli & Balaras (1999), and Gullbrand & Chow (2002) among others. Studies using three-dimensional filtering were performed by Cabot (1994), Gullbrand (2001), Winckelmans, Wray, Vasilyev & Jeanmart (2001), and Stolz, Adams & Kleiser (2001). However, most of the studies using three-dimensional filtering did not focus on minimizing the effect from the numerical errors. If care is not taken to reduce the errors, they may be larger than the contribution from the turbulence closure models. Therefore, it will not be possible to separate the effects from the numerics and the behavior of the turbulence closure models. Cabot (1994), for example, used a second-order finite-difference scheme and second-order filter functions with a ratio of two between the filter width and cell size. The error from the second-order scheme is probably larger than the turbulence closure contribution due to the small ratio of filter width to cell size used and, in addition, a second-order commutation error is present. Therefore, the LES results are highly affected by the numerical errors. Winckelmans *et al.* (2001) used a high-order finite-difference scheme (fourth-order) but applied a second-order filter with a ratio of filter width to cell size of $\sqrt{6}$. The use of a second-order filter introduces commutation errors of second-order which are of the same order as the turbulence model contribution in the simulations. A spectral method was used by Stolz *et al.* (2001), together with fourth-order commutative filter functions with a filter-grid ratio of approximately 1.5. The use of spectral methods clearly reduces the numerical errors in the simulation when compared to the studies previously mentioned. However, the use of explicit filtering in spectral methods is questionable. In spectral methods, the RSFS term can be exactly reconstructed from the filtered field, and truncation errors are not present in the small scales. Therefore, there is no need for explicit filtering when using spectral methods (Winckelmans & Jeanmart 2001). In addition, spectral methods can be applied only to specific geometries and cannot be used in flow fields of engineering interest, so they are not considered here. Gullbrand (2001) used fourth-order commutative filter functions, with a ratio of two between the filter width and cell size, in a fourth-order finite-difference code. The commutation error is then of the same order as the numerical scheme, which is of higher order than the turbulence closure contribution. According to the study by Chow & Moin (2003), the filter-grid ratio used ensures that the contribution from the turbulence closure term is larger than the numerical errors from the scheme. Thus, the fourth-order scheme using fourth-order commutative filters with a filter width of at least twice the cell size creates a numerically-clean environment where turbulence closure models can be tested and validated.

In this paper, turbulence closure models are evaluated using the "true" LES approach in turbulent channel flow. The study is an extension of the work presented by Gullbrand (2001), where fourth-order commutative filter functions are applied in three dimensions in a fourth-order finite-difference code. The true LES solution is the solution to the filtered governing equations. The solution is obtained by keeping the filter width constant while the computational grid is refined (figure 2). As the grid is refined, the solution will converge towards the true LES solution. The true LES solution will depend upon the filter width used, but be independent of the grid resolution. In traditional LES, because

the filter is implicit and directly connected to the grid spacing, the solution converges towards a direct numerical simulation (DNS) as the grid is refined, and not towards the filtered Navier-Stokes equations. The effect of turbulence closure models is therefore difficult to determine in traditional LES because, as the grid is refined, more length scales are resolved and less influence from the models is expected in the LES results. In contrast, in the true LES formulation, the explicit filter eliminates all scales that are smaller than the filter cutoff, regardless of the grid resolution. This ensures that the resolved length-scales do not vary as the grid resolution is changed. A resolution requirement for the true LES is that the cell size must be smaller than or equal to the cutoff length scale of the filter function.

The turbulence closure models investigated are the dynamic Smagorinsky model (DSM), the dynamic mixed model (DMM), and the dynamic reconstruction model (DRM). These turbulence models were previously studied using two-dimensional explicit filtering in turbulent channel flow by Gullbrand & Chow (2002). The DSM by Germano, Piomelli, Moin & Cabot (1991) is used as the USFS model in all the simulations, to be able to evaluate different reconstruction models for the RSFS stresses. The DMM (Zang, Street & Koseff 1993) consists of the scale-similarity model (SSM) by Bardina, Ferziger & Reynolds (1983), which is the RSFS model, in linear combination with the DSM. In the DRM, the RSFS stresses are modeled by using an estimate of the unfiltered velocity in the unclosed term, while the USFS stresses are modeled by the DSM.

2. Governing equations

The governing equations for an incompressible flow field are the continuity equation together with the Navier-Stokes equations,

$$\frac{\partial u_i}{\partial x_i} = 0 \,, \qquad \frac{\partial u_i}{\partial t} + \frac{\partial u_i u_j}{\partial x_j} = -\frac{\partial p}{\partial x_i} + \frac{1}{Re_\tau}\frac{\partial^2 u_i}{\partial x_j \partial x_j} \,. \tag{2.1}$$

Here u_i denotes velocity, p pressure and Re_τ the Reynolds number based upon friction velocity, u_τ, and channel half-width, h. Einstein summation is applied to repeated indices.

In LES, the governing equations are filtered in space. The filtering procedure is applied to the flow-field variables according to

$$\overline{u}_i(x,\Delta,t) = \int_{-\infty}^{\infty} G(x,x',\Delta) u_i(x',t) dx' \,, \tag{2.2}$$

where G is the filter function and Δ is the filter width.

Hence, the filtered governing equations can be written as

$$\frac{\partial \overline{u}_i}{\partial x_i} = 0 \,, \qquad \frac{\partial \overline{u}_i}{\partial t} + \frac{\partial \overline{\overline{u}_i}\overline{\overline{u}}_j}{\partial x_j} = \frac{\partial \overline{p}}{\partial x_i} + \frac{1}{Re_\tau}\frac{\partial^2 \overline{u}_i}{\partial x_j \partial x_j} - \frac{\partial \overline{\tau}_{ij}}{\partial x_j} \tag{2.3}$$

where the turbulent stresses are defined as $\overline{\tau}_{ij} = \overline{u_i u_j} - \overline{\overline{u}_i}\overline{\overline{u}}_j$. The filtered equations are not closed because of the nonlinear term $\overline{u_i u_j}$. Note that a second filtering is applied to the convective and turbulent stress terms (the nonlinear terms) in (2.3), to ensure that the wavenumber content is the same for every term in the equations. The product of the nonlinear terms ($\overline{u}_i\overline{u}_j$) introduces high wavenumbers that are beyond the wavenumber content of the filtered velocity field ($\overline{u}_i$). To prevent these high wavenumbers to influence the resolved wavenumbers, the nonlinear terms are explicitly filtered. A potential drawback of (2.3) is that the resulting equation is in general not Galilean-invariant. However, if an appropriate turbulence closure model is used, the problem can be avoided.

3. Subfilter-scale models

The turbulent flow field is divided into RFS motions and SFS motions when explicit filtering of the Navier-Stokes equations is applied. In figure 1, a sketch of a typical energy spectrum is shown. The solid line represents the energy captured by a fully resolved DNS, while the dashed line represents the LES energy. The vertical line at k_{cg} shows the filter cutoff in the LES. The filter cutoff is determined by where the filter function goes to zero and stays zero (in spectral space), *i.e.* no wavenumbers higher than the cutoff wavenumber are resolved in the simulation. The filter cutoff can be seen in figure 2. All wavenumbers smaller than the filter cutoff wavenumber are resolved in the simulations. However, they are damped by the filter function and have to be recovered by an inverse filter operation. This corresponds to the RSFS portion of the energy spectrum. The same terminology for the RSFS and the USFS was previously suggested by Zhou *et al.* (2001). In theory, the RSFS can be exactly recovered, but this is only possible when using spectral methods. If non-spectral methods are applied, there are numerical errors (NE) associated with the high wavenumbers and thus the recovered scales are contaminated with errors. The unresolved portion of the spectrum (the USFS) consists of wavenumbers that are higher than the filter cutoff wavenumber. The USFS motions need to be modeled. The USFS portion of the spectrum was previously called the subgrid-scale (SGS) portion in the study by Gullbrand & Chow (2002). However, the name is not valid here, since it is the filter function that determines the cutoff location and not the computational grid. The vertical lines in the figure represent the grid cutoff wavenumbers for two grid resolutions. The coarse grid cutoff, k_{cg}, happens to coincide with the filter cutoff, while the fine grid cutoff, k_{fg}, is located in the USFS portion of the spectrum. However, the USFS motions are the same in the two simulations, since the filter cutoff determines the wavenumbers resolved.

To recover the RSFS stresses, the iterative method of van Cittert (1931) is used in this study. This method was previously used by Stolz *et al.* (2001) in their approximate deconvolution procedure to reconstruct the unfiltered velocity field u_i from the filtered field $\overline{u}_i$. To fully recover the unfiltered velocity, an infinite number of iterations is needed. However, since this is not practical in numerical simulations, the unfiltered velocity field is approximated by a finite number of iterations. By varying this number, different models can be obtained to model the RSFS stresses.

Here, low-level reconstruction (the SSM) and reconstruction of level five using the approximate deconvolution model (ADM) by Stolz *et al.* (2001) are used to model the RSFS stresses. Further details of the reconstruction used are found in 3.3. In order to compare the different RSFS models, the same USFS model (the DSM) is used in all the simulations. The combinations of RSFS and USFS models used are described below.

3.1. *Dynamic Smagorinsky Model*

The DSM is a widely-used eddy viscosity USFS model (Smagorinsky 1963):

$$\overline{\tau}_{ij} = -2\overline{\nu_e \overline{S}}_{ij} = -2\overline{(C\Delta)^2 |\overline{S}| \overline{S}}_{ij}, \tag{3.1}$$

where ν_e is the eddy viscosity, Δ the filter width and S_{ij} the strain rate tensor. The model parameter $(C\Delta)^2$ is calculated dynamically (Germano *et al.* 1991) using the least-square approximation of Lilly (1992). The model parameter is calculated by the same dynamic procedure as described in the papers previously mentioned. The explicit filtering of the nonlinear terms is not considered when the model parameter is calculated. The filtering

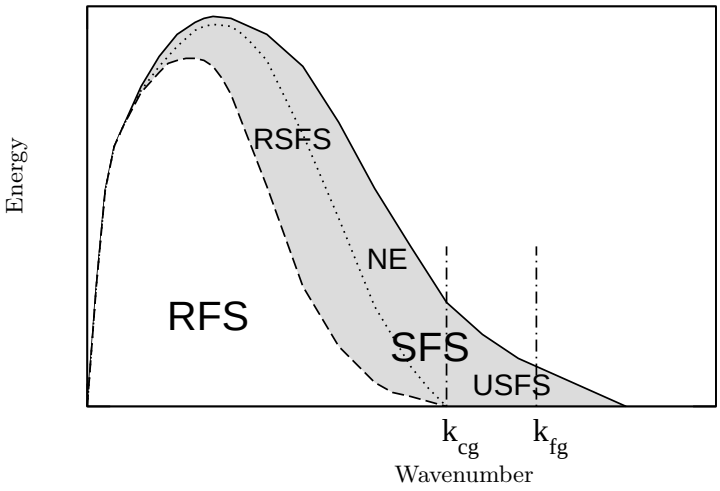

FIGURE 1. Schematic of velocity energy spectrum showing partitioning into resolved filtered scale (RFS), resolved subfilter-scale (RSFS), and unresolved subfilter-scale (USFS) motions. The numerical error (NE) region, denoted by ····· , is a subregion of the RSFS. ——— represents DNS energy, - - - - LES energy, and —·— filter cutoff. The vertical line at k_{cg} represents the filter cutoff wavenumber, which corresponds to the smallest resolved wavenumber for the coarse grid. The vertical line at k_{fg} represents the wavenumber cutoff for the fine grid.

enters only in the final stage of the process, when τ_{ij} is introduced into the filtered Navier-Stokes equations.

3.2. *Dynamic Mixed Model*

Low-level reconstruction of the RSFS stresses can be performed by using the scale-similarity model proposed by Bardina *et al.* (1983). The SSM is obtained by substituting $u_i \approx \overline{u}_i$ into the definition of the turbulence stress tensor, $\overline{\tau}_{ij}$. Here the RSFS stress is modeled by the scale-similarity term and the DSM is used as the USFS model:

$$\overline{\tau}_{ij} = (\overline{\overline{u}_i\overline{u}_j} - \overline{\overline{u}_i}\,\overline{\overline{u}_j}) - 2\overline{(C\Delta)^2|\overline{S}|\overline{S}}_{ij}\,, \tag{3.2}$$

to form the DMM. In the code, the SSM term is discretized with the same numerical scheme as the convective terms.

3.3. *Dynamic Reconstruction Model*

High-order reconstruction of the RSFS stress tensor can be achieved by the iterative deconvolution method of van Cittert (1931). The unfiltered quantities can be derived by a series of successive filtering operations (G) applied to the filtered quantities with

$$u_i = \overline{u}_i + (I - G) * \overline{u}_i + (I - G) * ((I - G) * \overline{u}_i) + \cdots \tag{3.3}$$

where I is the identity matrix. The truncation order of the expansion determines the level of deconvolution, as discussed by Stolz *et al.* (2001). If the series includes the terms explicitly shown in (3.3), it corresponds to reconstruction of level two. An approximate unfiltered velocity ($u_i^\star$) is obtained by the truncated series. $u_i^\star$ is substituted into the unclosed term $\overline{u_iu_j}$, which results in $\overline{u_i^\star u_j^\star}$. This reconstruction was used by Stolz *et al.*

(2001) to form the ADM. Here the ADM is used in linear combination with the DSM,

$$\overline{\tau}_{ij} = \overline{u_i^\star u_j^\star} - \overline{\overline{u}_i \overline{u}_j} - 2\overline{(C\Delta)^2 |\overline{S}| \overline{S}}_{ij} \ , \tag{3.4}$$

which is called the dynamic reconstruction model (DRM). In the simulations, the same numerical scheme is used for the convective terms and the RSFS terms. The DRM yields a Galilean-invariant expression of (2.3), since the nonlinear terms $\overline{\overline{u}_i \overline{u}_j}$ on the right-hand side and left-hand side of the equation cancel each other. A reconstruction series of level five is used in this study.

4. Filter functions

It is important that the explicit filter and the test filter, which is used in the dynamic procedure of the DSM, have similar shapes, since the dynamic procedure is based upon the scale-similarity assumption in the Germano identity (Germano *et al.* 1991). In the simulations presented here, the same filter function is used in all the simulations. It is only the filter width that is varied between the simulations. The base filter is a fourth-order commutative filter function with filter width $2\Delta_{cg}$, where Δ_{cg} is the grid cell size for the coarse-grid resolution. The computational domain and grid resolutions used in the simulations are discussed in section 6. It is not straightforward to determine the filter width of a high-order filter and different methods were studied by Lund (1997). Here, one of the methods suggested by Lund is applied. The filter width is defined as the location where the filter function reaches a value of $G(k) = 0.5$. The filter function used in the simulations was developed by Vasilyev *et al.* (1998) and is

$$\overline{\phi}_i = -\frac{1}{32}\phi_{i-3} + \frac{9}{32}\phi_{i-1} + \frac{1}{2}\phi_i + \frac{9}{32}\phi_{i+1} - \frac{1}{32}\phi_{i+3}, \tag{4.1}$$

where the filter weights for $\phi_{i\pm2}$ are zero. The smooth filter function is shown in spectral space in figure 2. In the near-wall region, asymmetric filters are used in the first three grid points for the coarse grid in the wall-normal direction.

In the simulations, the ratio of the test-filter width to the explicit-filter width is chosen to be two, as proposed by Germano *et al.* (1991) for the DSM. The test filter is used only in the calculation of $(C\Delta)^2$ in the DSM, while the explicit filter function is used to determine the RSFS contribution through either the SSM or the ADM. The ratio between the explicit-filter width and the cell size for the coarse grid is two and for the fine grid (128,97,96), the ratio is four. This preserves the effective filter width as the grid resolution is increased, as seen in figure 2. The vertical line at low wavenumber represents the grid cutoff (k_{cg}) for the coarse-grid resolution. The filter cutoff wavenumber is the same as the grid cutoff for the coarse grid. For the fine grid, the filter cutoff is held fixed, resulting in a separation between the filter cutoff and grid cutoff (k_{fg}) locations. The grid-cutoff wavenumbers are also shown schematically in figure 1. The ratio of two between the filter width and the cell size for the coarse grid was chosen to prevent the numerical error from the finite-difference scheme from becoming larger than the contribution of the turbulence closure model (Ghosal 1996; Chow & Moin 2003).

5. Solution algorithm

In the computational code, the spatial derivatives are discretized using a fourth-order central-difference scheme on a staggered grid. The convective term is discretized in the skew-symmetric form (Morinishi, Lund, Vasilyev & Moin 1998; Vasilyev 2000) to ensure

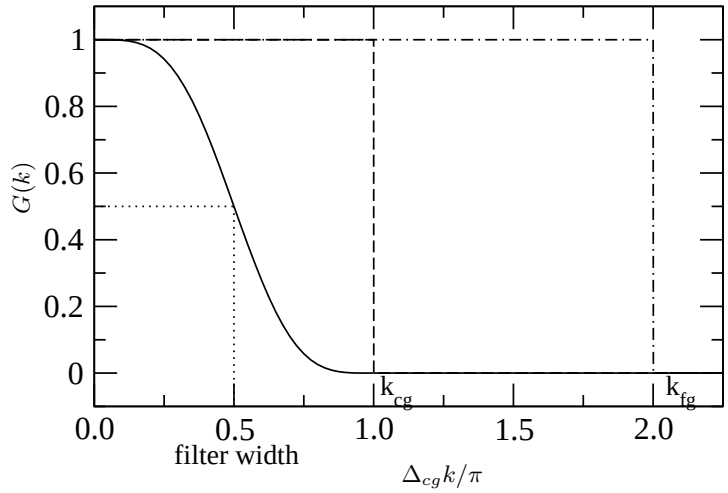

FIGURE 2. The base filter function in spectral space and its relation to the computational grid resolutions. ——— : filter function, ····· : filter width, – – – – : coarse grid resolution, and —·— : fine grid resolution. The wavenumber k_{cg} represents the grid cutoff wavenumber for the coarse grid, while k_{fg} represents the grid cutoff wavenumber for the fine grid.

conservation of turbulent kinetic energy. The equations are integrated in time using the third-order Runge-Kutta scheme described by Spalart, Moser & Rogers (1991). The diffusion terms in the wall-normal direction are treated implicitly by the Crank-Nicolson scheme. The splitting method of Dukowicz & Dvinsky (1992) is used to enforce the solenoidal condition. The resulting discrete Poisson equation for the pressure is solved in the wall-normal direction using a pentadiagonal matrix solver. In the homogeneous directions, the Poisson equation is solved using a discrete Fourier transform. Periodic boundary conditions are applied in the streamwise and spanwise homogeneous directions, with no-slip conditions at the channel walls. A fixed mean pressure gradient is used to drive the flow. The computational code is compared to a second-order finite-difference code in Gullbrand (2000) and Gullbrand & Chow (2002).

6. Turbulent channel flow simulations

The Reynolds number is $Re_\tau = 395$ and the computational domain is $(2\pi h, 2h, \pi h)$ in (x, y, z) where x is the streamwise direction, y the wall-normal direction, and z the spanwise direction. The computational grid is stretched in the y-direction by a hyperbolic tangent function

$$y(j) = -\frac{\tanh(\gamma(1 - 2j/N_2))}{\tanh(\gamma)} \qquad j = 0, ..., N_2 \tag{6.1}$$

where N_2 is the number of grid points in the wall-normal (j) direction and γ is the stretching parameter, which is set to 2.75. Two computational grids are used; (64,49,48), which corresponds to one-quarter of the DNS resolution in each spatial direction, and (128,97,96), which is half the number of DNS grid points in each direction. The cell size for the coarser grid resolution is $\Delta x^+ = 39$, $\Delta z^+ = 26$, and $0.4 \leq \Delta y^+ \leq 45$. The finer resolution corresponds to the cell size $\Delta x^+ = 19$, $\Delta z^+ = 13$, and $0.2 \leq \Delta y^+ \leq 23$. The 'plus' values (wall units) are obtained by normalizing the length scale with the friction

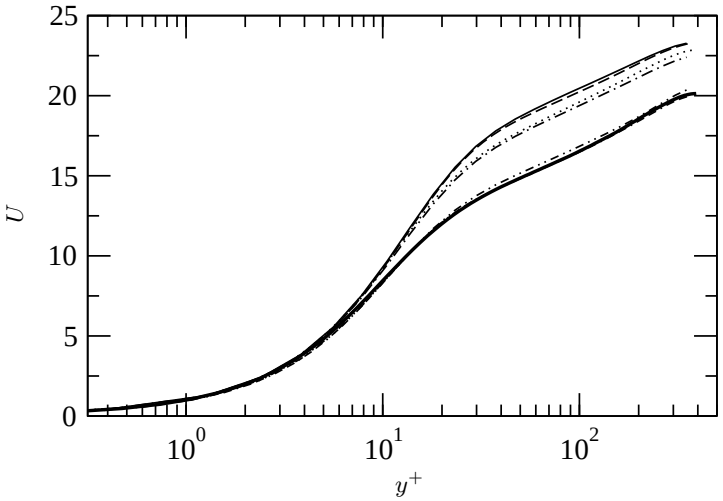

FIGURE 3. Mean velocity profiles using different turbulence closure models. ——— : DNS, ——— : DSM (64,49,48), – – – – : DSM (128,97,96), —·— : DMM (64,49,48), ····· : DMM (128,97,96), —··— : DRM (64,49,48), and ·——· : DRM (128,97,96).

velocity and the kinematic viscosity (ν). A statistically stationary solution is obtained after 30 dimensionless time units, and thereafter statistics are sampled during 15 time units. The time is normalized with the friction velocity and channel half-width. The LES results are compared to the unfiltered DNS data of Moser, Kim & Mansour (1999).

7. Results

Figure 3 shows mean velocity profiles from simulations using different RSFS models and different grid resolutions. The filter width is fixed, while the grid resolution is increased. The goal is to obtain a grid-independent LES solution so that the behavior of turbulence closure models can be evaluated. The changes in the predicted mean velocity profiles as the grid resolution is increased are only minor, indicating that the LES solutions are converged. The mean velocities predicted by the DSM are much higher than the DNS results. The DMM improves the results slightly, while the best agreement with the DNS data is predicted by the DRM. This shows the need for a RSFS model when a smooth explicit filter function is applied.

The streamwise velocity fluctuations in figure 4 show the same trend as the mean velocity profiles. However, the differences in the results as the grid is refined are slightly larger than for the mean velocity. The DSM shows the largest overprediction of the peak streamwise velocity fluctuations. The peak value decreases slightly as the grid is refined. This is also observed for the DMM and the DRM. It should be noted that the DRM actually predicts a peak value that is lower than the DNS data. This is very unusual in LES, because most models will overpredict the streamwise velocity fluctuations and underpredict the wall-normal and spanwise fluctuations. However, an underprediction of all velocity fluctuations is to be expected in LES, since LES can be considered as filtered DNS, and if the DNS results filtered, the peak values are expected to decrease.

As pointed out by Winckelmans, Jeanmart & Carati (2002), when LES turbulence intensities (or velocity fluctuations) are compared to DNS data, the LES intensities should

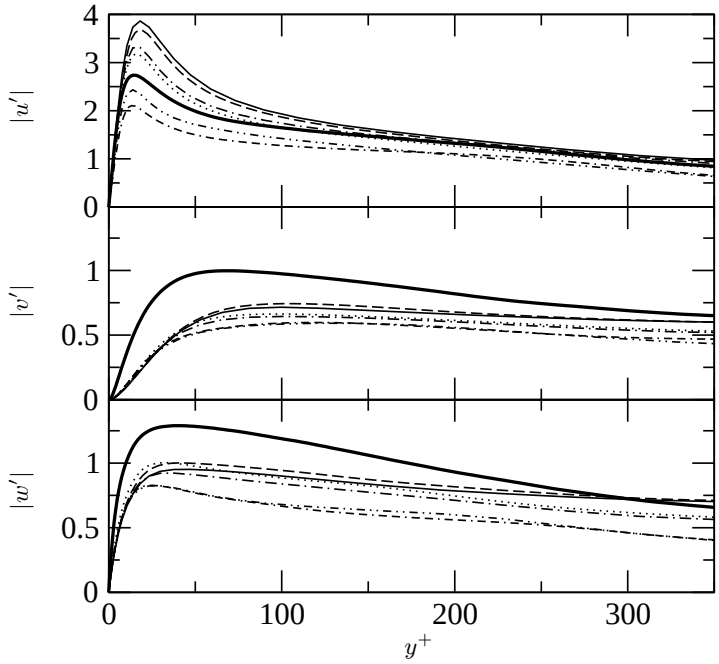

FIGURE 4. Velocity fluctuations in the streamwise $|u'|$, wall-normal $|v'|$, and spanwise $|w'|$ directions. ——— : DNS, ——— : DSM (64,49,48), – – – – : DSM (128,97,96), —·— : DMM (64,49,48), ····· : DMM (128,97,96), —··— : DRM (64,49,48), and ·——— : DRM (128,97,96).

include the contribution from the turbulence closure models. However, if a traceless turbulence model like the DSM, or partially-traceless models as the DMM and DRM, are used, it is only the reduced (deviatoric) turbulence intensities of both the DNS and the LES that should be compared. The reduced intensities represent the deviation from isotropy, and the streamwise turbulence intensities are given by

$$-R_{xx} = u'u' - 1/3(u'u' + v'v' + w'w').$$

The reduced turbulence intensities are compared in figure 5. In this paper, both the turbulence intensities and the velocity fluctuations are studied. The reason for investigating both quantities is to show that incorrect conclusions may have been made in previous studies concerning model behavior, since it is usually the uncorrected velocity fluctuations that are compared. As observed in figure 5, the magnitudes of the turbulence intensities show a consistent behavior for all three intensities. The DSM shows the largest overprediction of the peak value. The DMM decreases the predicted peak values slightly, while the DRM predicts peak values that are lower than the DNS. As mentioned earlier, an underprediction of the peak value is expected in LES. When the grid is refined, the peak values decrease slightly for all the models studied. The behavior of the turbulence intensities is not consistent with the observations made for the velocity fluctuations. For the wall-normal and spanwise velocity fluctuations, the DSM predictions are closer to the DNS data than the other models. The DRM predicts velocity fluctuations that are lower than the DNS data in the streamwise direction, while the results in the wall-normal and the spanwise directions show the largest deviation of the models from the DNS re-

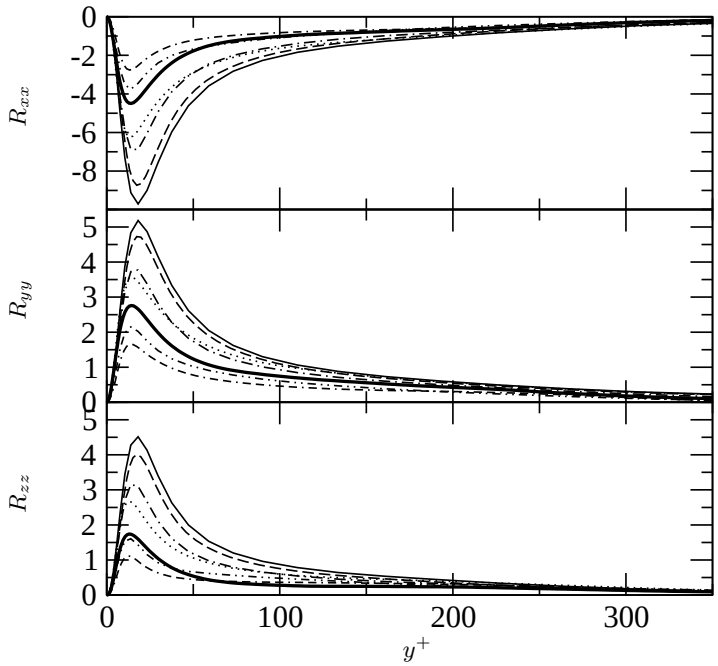

FIGURE 5. Reduced (deviatoric) turbulence intensities in streamwise R_{xx}, wall-normal R_{yy}, and spanwise R_{zz} directions. ——— : DNS, ——— : DSM (64,49,48), - - - - : DSM (128,97,96), —·— : DMM (64,49,48), ····· : DMM (128,97,96), —··— : DRM (64,49,48), and ·——· : DRM (128,97,96).

sults. The velocity fluctuations therefore seem to give a rather confusing message of the DRM behavior, while the turbulence intensities show a consistent behavior for all three intensities.

The modeled shear stresses are shown in figure 6. It is a well-known problem that the DSM does not predict enough shear stress in the near-wall region (Baggett, Jimenez & Kravchenko 1997). As shown in the figure, the total modeled shear stress increases as the level of reconstruction is increased. However, the contribution from the DSM does not change much between the different simulations; the peak value is approximately the same. The increase of modeled shear stress is therefore almost entirely due to the RSFS model.

8. Discussion and conclusions

The true LES approach is investigated in turbulent channel flow using commutative filter functions in all three spatial directions. In the true LES approach, a grid-independent solution to the filtered governing equations is obtained. A computational code using an energy-conserving fourth-order finite-difference scheme is applied and fourth-order commutative filters are used. Simulations of turbulent channel flow were performed at $Re_\tau = 395$. The explicit filter width was kept fixed while the computational grid was refined, to obtain a grid-independent solution. The results using two different grid resolutions show only minor differences, indicating that the LES solutions are converged. The explicit filtering also reduces the numerical errors that are associated with the high-

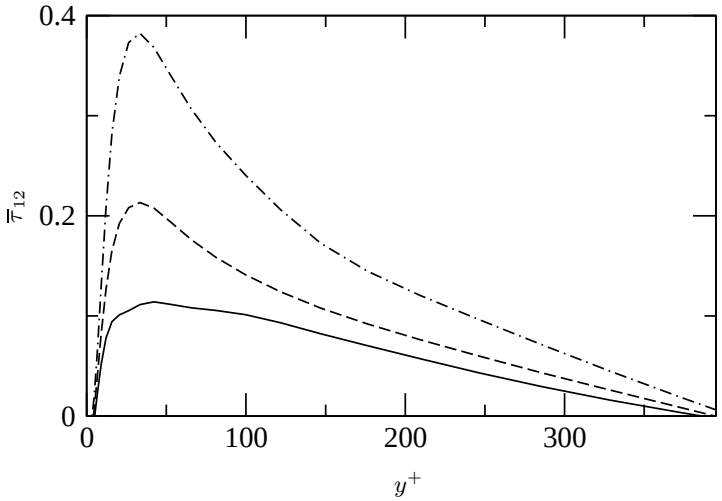

FIGURE 6. Modeled shear stress, $\overline{\tau}_{12}$, using different turbulence closure models for the computational grid (64,49,48). ——— : DSM, - - - - : DMM, —·— : DRM.

wavenumber portion of the spectrum when using non-spectral methods. Therefore, explicit filtering in LES, using high-order commutative filters, results in a numerically-clean environment where turbulence closure models can be investigated in grid-independent LES solutions.

The turbulence closure models investigated are the DSM, DMM and DRM. The models are compared to DNS data for mean velocity profiles, velocity fluctuations, and reduced turbulence intensities. The results show that since the turbulence closure models are traceless (the DSM) or partially traceless (the DMM and the DRM), special care is needed when comparing the turbulence quantities to DNS results. The reduced turbulence intensities represent the deviation from isotropy and show a consistent behavior of the models, while these conclusions cannot be drawn from studying the velocity fluctuations.

The poor agreement between the DNS results and the DSM shows the need for RSFS models when a smooth (in spectral space) explicit filter function is applied. In theory, the RSFS stresses can be exactly reconstructed by an inverse-filtering operation. However, in a non-spectral method, the RSFS stresses cannot be exactly reconstructed, due to numerical errors. The results predicted by the models investigated show a distinct improvement in the predicted quantities, when compared to DNS results, as the level of reconstruction is increased. These improvements are probably due to the increase of modeled shear stress in the near-wall region. The DSM is known not to predict enough shear stress in the near-wall region, and as the level of reconstruction is increased so is the modeled shear stress. The increase is almost entirely due to the RSFS model, since the contribution from the DSM does not change much in the simulations. However, it should be noted that even if an exact reconstruction of the RSFS stresses can be obtained, the results will depend on the USFS model used. The LES results need to be compared to filtered DNS data, since the governing equations are filtered. The accuracy of using the DSM to capture the USFS stresses also needs to be determined.

Acknowledgments

Thanks are extended to Profs. P. Moin and O. V. Vasilyev who contributed through many helpful discussions. Thanks are also due to F. K. Chow for her input.

REFERENCES

Baggett, J., Jimenez, J. & Kravchenko, A. G. 1997 Resolution requirements in large-eddy simulations of shear flows. *Annual Research Briefs*, Center for Turbulence Research, NASA Ames/Stanford Univ., 51–66.

Bardina, J., Ferziger, J. H. & Reynolds, W. C. 1983 Improved turbulence models based on large eddy simulation of homogeneous, incompressible, turbulent flows. *Tech. Rept.* TF-19, Mech. Engg. Dept., Stanford Univ.

Cabot, W. 1994 Local dynamic subgrid-scale models in channel flow. *Annual Research Briefs*, Center for Turbulence Research, NASA Ames/Stanford Univ., 143–159.

Carati, D., Winckelmans, G. & Jeanmart, H. 2001 On the modelling of the subgrid-scale and filtered-scale stress tensors in large-eddy simulation. *J. Fluid Mech.* **441**, 119–138.

Chow, F. K. & Moin, P. 2003 A further study of numerical errors in large-eddy simulations. To appear in *J. Comp. Phys.*

van Cittert, P. 1931 Zum Einfluß der Spaltbreite auf die Intensitätsverteilung in Spektrallinien II. *Zeit. für Physik* **69**, 298–308.

Dukowicz, J. & Dvinsky, A. 1992 Approximate factorization as a high-order splitting for the implicit incompressible-flow equations. *Journal of Computational Physics* **102** (2), 336–347.

Germano, M., Piomelli, U., Moin, P. & Cabot, W. 1991 A dynamic subgrid-scale eddy viscosity model. *Phys. Fluids* **3** (7), 1760–1765.

Ghosal, S. 1996 An analysis of numerical errors in large-eddy simulations of turbulence. *J. Comp. Phys.* **125**, 187–206.

Ghosal, S. & Moin, P. 1995 The basic equations for the large eddy simulation of turbulent flows in complex geometry. *J. Comp. Phys.* **118**, 24–37.

Gullbrand, J. 2000 An evaluation of a conservative fourth order dns code in turbulent channel flow. *Annual Research Briefs*, Center for Turbulence Research, NASA Ames/Stanford Univ., 211–218

Gullbrand, J. 2001 Explicit filtering and subgrid-scale models in turbulent channel flow. *Annual Research Briefs*, Center for Turbulence Research, NASA Ames/Stanford Univ., 31–43.

Gullbrand, J. & Chow, F. 2002 Investigation of numerical errors, subfilter-scale models, and subgrid-scale models in turbulent channel flow simulations. Proceedings of the Summer Program. Center for Turbulence Research, NASA Ames/Stanford Univ.,

Lilly, D. 1992 A proposed modification of the Germano subgrid-scale closure method. *Phys. Fluids* **4**, 633–635.

Lund, T. S. 1997 On the use of discrete filters for large eddy simulation. *Annual Research Briefs*, Center for Turbulence Research, NASA Ames/Stanford Univ., 83–95.

Morinishi, Y., Lund, T., Vasilyev, O. & Moin, P. 1998 Fully conservative higher order finite difference schemes for incompressible flow. *J. Comp. Phys.* **143**, 90–124.

Moser, R., Kim, J. & Mansour, N. 1999 Direct numerical simulation of turbulent channel flow up to $Re_\tau = 590$. *Phys. Fluids* **11**, 943–945.

Najjar, F. & Tafti, D. 1996 Study of discrete test filters and finite difference approximations for the dynamic subgrid-scale stress model. *Phys. Fluids* **8**, 1076–1088.

Piomelli, U., Moin, P. & Ferziger, J. 1988 Model consistency in large eddy simulation of turbulent channel flows. *Phys. Fluids* **31**, 1884–1891.

Sarghini, F., Piomelli, U. & Balaras, E. 1999 Scale-similar models for large-eddy simulations. *Phys. Fluids* **11**, 1596–1607.

Smagorinsky, J. 1963 General circulation experiments with the primitive equations. *Mon. Weather Rev.* **91**, 99–152.

Spalart, P., Moser, R. & Rogers, M. 1991 Spectral methods for the navier-stokes equations with one infinite and 2 periodic directions. *J. Comp. Phys.* **96**, 297–324.

Stolz, S., Adams, N. & Kleiser, L. 2001 An approximate deconvolution model for large-eddy simulation with application to incompressible wall-bounded flows. *Phys. Fluids* **13**, 997–1015.

Vasilyev, O. 2000 High order finite difference schemes on non-uniform meshes with good conservation properties. *J. Comp. Phys.* **157**, 746–761.

Vasilyev, O., Lund, T. & Moin, P. 1998 A general class of commutative filters for les in complex geometries. *J. Comp. Phys.* **146**, 82–104.

Winckelmans, G. & Jeanmart, H. 2001 Assessment of some models for les without/with explicit filtering. In *Direct and Large-Eddy Simulation IV* (B. Geurts, F. Friedrich & O. Métais, eds.), Kluwer, Dordrecht, 55-66.

Winckelmans, G., Jeanmart, H. & Carati, D. 2002 On the comparison of turbulence intensities from large-eddy simulation with those from experiment or direct numerical simulation. *Phys. Fluids* **14**, 1809–1811.

Winckelmans, G., Wray, A., Vasilyev, O. & Jeanmart, H. 2001 Explicit-filtering large-eddy simulation using the tensor-diffusivity model supplemented by a dynamic smagorinsky term. *Phys. Fluids* **13** (5), 1385–1403.

Zang, Y., Street, R. L. & Koseff, J. R. 1993 A dynamic mixed subgrid-scale model and its application to turbulent recirculating flows. *Phys. Fluids* **5**, 3186–3196.

Zhou, Y., Brasseur, J. & Juneja, A. 2001 A resolvable subfilter-scale model specific to large-eddy simulation of under-resolved turbulence. *Phys. Fluids* **13**, 2602–2610.